In situ investigation of the early stage of TiO$_2$ epitaxy on (001) SrTiO$_3$

M. Radović,[1,2,a)] M. Salluzzo,[2,3] Z. Ristić,[2,4] R. Di Capua,[2,5] N. Lampis,[2,6] R. Vaglio,[2,3] and F. Miletto Granozio[2,3]

[1]*LSNS - EPFL, PH A2 354 (Bâtiment PH) Station 3 CH-1015 Lausanne, Switzerland*
[2]*CNR-SPIN, Complesso Universitario Monte S. Angelo, Via Cintia I-80126 Napoli, Italy*
[3]*Dipartimento di Fisica, Università "Federico II" di Napoli, Piazzale Tecchio, I-80126, Italy*
[4]*Département de Physique de la Matière Condensée, University of Geneva, 24 Quai Ernest-Ansermet, CH-1211 Geneva 4, Switzerland*
[5]*Dipartimento S.pe.S., Università degli Studi del Molise - Via De Sanctis, I-86100 Campobasso, Italy*
[6]*Laborvetro srl, via Calamattia 6, I-09134 Cagliari, Italy*

We report on a systematic study of the growth of epitaxial TiO$_2$ films deposited by pulsed laser deposition on Ti-terminated SrTiO$_3$ (001) single crystals. By using *in situ* reflection high energy electron diffraction, low energy electron diffraction, x-ray photoemission spectroscopy, and scanning probe microscopy, we show that the stabilization of the anatase (001) phase is preceded by the growth of a few nanometers thick pseudomorphic Sr$_x$TiO$_{2+y}$ (x, y < 1) intermediate layer. The data demonstrate that the formation of this intermediate phase is related to the activation of a long range Sr migration from the SrTiO$_3$ substrate into the film. Our results enrich the phase diagram of the Sr–Ti–O system under epitaxial strain opening a route for the study of the electronic and dielectric properties of the reported Sr-deficient SrTiO$_3$ phase. © *2011 American Institute of Physics*. [doi:10.1063/1.3613637]

INTRODUCTION

In recent years, oxide interfaces have generated a substantial interest due to novel functionalities that are not present in the single constituting layers. A widely celebrated example is provided by the discovery of a two-dimensional (2D) electron gas at the LaAlO$_3$/SrTiO$_3$ interface.[1] The exciting novel properties of this system are explained in terms of a purely "electronic reconstruction" mechanism.[2,3] Extrinsic doping caused by point defects might, however, occur at the interface. In this framework, cation disorder at the SrTiO$_3$ (STO) surface is a central issue. Cation interdiffusion in all-perovskite heterostructures is in general modest, and recent data set a single atomic plane as the upper limit on the distance for cation migration.[4] Intermixing or atomic roughening of the interfaces, even at the level of a single atomic plane, can nevertheless affect the functional properties of these systems.[5] More generally speaking, the early stages of the growth of oxide thin films on STO single crystals are of very wide interest, and it is crucial to determine whether Sr inter-diffusion may occur during the film growth.

In this paper, we present a detailed study of the early stages of the growth of anatase TiO$_2$ (001) thin films deposited by pulsed laser deposition (PLD) on TiO$_2$ terminated SrTiO$_3$ (001) single crystals. This heterostructure can be accepted as appropriate model to study Sr inter-diffusion that may occur under the presence of tensile strain. Furthermore, the choice of TiO$_2$ films was motivated by the large interest of this material in applications, and in particular in photocatalysis,[6] solar cells,[7] gas sensors,[8] photovoltaics,[9] and more recently, spintronics devices.[10] While the growth of both anatase and rutile TiO$_2$ films was successfully achieved on LaAlO$_3$ (Ref. 11) and untreated SrTiO$_3$ (Ref. 12) substrates, a thorough investigation of the early stage of growth of this material on well-ordered TiO$_2$ terminated STO, to our knowledge, was not accomplished until now.

The ideal crystal structure of epitaxial TiO$_2$/SrTiO$_3$ system is shown in Fig. 1(a). STO (001) is composed of a vertical stack of alternating SrO (A-type) and TiO$_2$ (B-type) planes. The TiO$_2$ planes in STO are flat and undistorted, with 0.3905 nm lattice spacing. They are in tensile strain, due to the intercalated SrO planes, a circumstance that makes STO an incipient ferroelectric.[13] The anatase phase of TiO$_2$ is instead composed of a vertical stack of alternating TiO$_2$ (B-type) planes. The TiO$_6$ octahedra in the anatase structure are distorted and rotated with respect to each other. Consequently, every TiO$_2$ plane is strongly buckled (with a O-Ti-O bond angle $\alpha \approx 156°$).

The lattice mismatch between anatase TiO$_2$ (001) and STO (001) amounts to 3.1% (Table I) and epitaxial films are expected to be under a tensile strain. Due to this large lattice mismatch, a coherent anatase TiO$_2$(001)/STO(001) interface, implying straightening and stretching of the Ti–O bonds,[14] has a high cost in terms of elastic energy and its stability is obviously questionable. Several strain-relief mechanisms can take place, including the relaxation of the TiO$_2$ layers by island growth, induction of oxygen non-stoichiometry, cation interdiffusion, or others. For instance, it has been reported that the interface between TiO$_2$ and STO has a cubic rock-salt crystal structure (TiO$_y$), with lattice parameters equal to 0.4 nm and oxygen content (y) between 0.58 and 1.33.[15] Weng *et al.*[15] suggest that this phase, which occurs during the initial stage of the film growth, is caused by a thermal treatment before the film deposition.
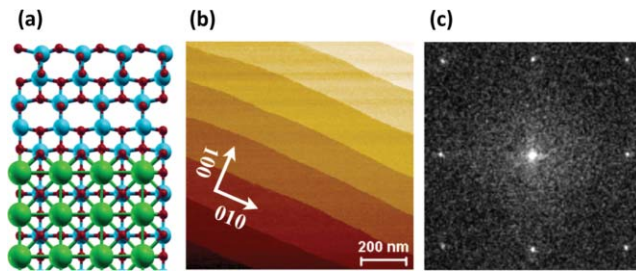
---

a)Electronic mail: milan.radovic@psi.ch.

135, 034705-1

FIG. 1. Ideal structure of strained anatase TiO_2 (001) film on TiO_2-terminated $SrTiO_3$ single crystal (Sr ions are green spheres, Ti are cyan, and oxygen ions are in red). (b) *In situ* non-contact AFM surface topography of our Ti-terminated STO substrates. (c) LEED pattern of single terminated samples.

Besides oxygen stoichiometry, cation interdiffusion across multiple layers could also play a crucial role in anatase/perovskite heterostructures. This is opposite to all-perovskite heterostructures, where a long-range diffusion of large cations (as A-site La or Sr) through interstitial sites is typically inhibited. Additionally, we notice that A-site cation intermixing between two stoichiometric perovskites requires the double exchange of A-type cations, which can be considered to some extent as a "second order" process. For this reason, the properties of perovskite oxide interfaces are in general affected by the more energetically favorable formation of oxygen vacancies.[16] On the other hand, the interlayer diffusion from the A-type sub-lattice of STO into the anatase lattice might be favored both by entropy and strain minimization and should be taken in account as a "first order" process.

On the basis of these qualitative considerations, it can be argued that interdiffusion of Sr ions into TiO_2 is a likely process. Therefore, it might either induce the formation of an inhomogeneous, phase-separated film, or favor the epitaxial growth of a non-stoichiometric pseudomorphic Sr-deficient Sr_xTiO_{2+y} phase (x, y < 1). The latter possibility is very interesting, since the phase diagram of the Sr–Ti–O system does not contain any thermodynamic phase with a [Sr]/[Ti] ratios lower than one.[17] Additionally, exploring the electronic properties of the system in the unexplored Sr-deficient region of the phase diagram near the $SrTiO_3$ phase can be interesting for tailoring the STO properties in view of specific applications.

In the following, we report on a comprehensive all *in situ* study of the earliest stages of growth of TiO_2 on STO single crystals. The results presented here show that an intermediate, Sr-deficient, strain-stabilized, perovskite-like phase with a thickness extending up to 2–4 nm can develop at the TiO_2/STO interface in controlled growth conditions. The

formation of such phase corresponds to the self-organization of the interstitial Sr, diffused into the epitaxially strained TiO_2, in a partially filled A-site sublattice. Such behavior is not found when TiO_2 films are deposited on other substrates, such as $LaAlO_3$ (LAO) and $SrLaAlO_4$ (SLAO), where anatase grows without or under slightly compressive strain (–0.8%) [Table I]. The realization of this phase is confirmed by detailed *ex situ* microscopic and compositional analysis.[18]

EXPERIMENTAL RESULTS

The multi-chamber ultra high vacuum (UHV) apparatus employed in this work was specifically designed for pulsed laser deposition of epitaxial oxide thin films and multilayers and for the analysis of the structural and electronic properties of the fresh uncontaminated surfaces of as-grown samples. It includes: (i) an UHV PLD setup equipped with a KrF excimer laser and a 30 keV high pressure RHEED; (ii) an analytical chamber dedicated to photoemission (XPS, UPS), low energy electron diffraction (spot profile analysis LEED), and scanning probe microscopy (SPM) and spectroscopy analyses. TiO_2 ultra-thin films were grown on (001) oriented $SrTiO_3$, $SrLaAlO_4$ (SLAO), and $LaAlO_3$ (LAO) single crystals and analyzed *in situ*, resorting to the above-mentioned complementary surface science techniques. In the case of STO single crystals, we employed both untreated (equally SrO and TiO_2 terminated) and single TiO_2 terminated substrates. The latter were prepared following a well-established etching procedure,[19] and subsequently annealed *in situ* in the PLD chamber in 0.1 mbar of O_2 at 950 °C for 2 h right before deposition. The *in situ* annealing procedure was adopted to reduce the risk of any possible surface contamination. RHEED, LEED, AFM, and surface diffraction analyses[20] of these single crystals demonstrate their high quality and a single termination [Fig. 1(b)–1(d)].

TiO_2 films were grown by PLD in flowing 0.1 mbar of molecular oxygen using a stoichiometric ceramic TiO_2 target, typical laser fluencies of 2.5 J/cm^2, and substrate temperatures of 800 °C. Some test samples were also deposited at different temperatures in the 650 °C–800 °C range, yielding substantially similar results. One sample intentionally was grown at room temperature for reference. Grazing incidence x-ray diffraction was used to calibrate the deposition rate of TiO_2 in our typical deposition conditions, which corresponds to about 55 pulses/nm or, equivalently, about 14 pulses/TiO_2 monolayer. Further data are also reported in Ref. 21. Films deposited on LAO and SLAO exhibit the typical (4 × 1) surface reconstruction of anatase TiO_2 (001) films.[22] These samples exhibit a high degree of crystallographic perfection

TABLE I. Calculated mismatch between anatase (001) TiO_2 (the plane lattice parameter is 0.3785 nm) and (001) STO, SLAO, and LAO substrates; The values of t_0 are found by fitting according to Eq. (1) for films deposited on different substrates.

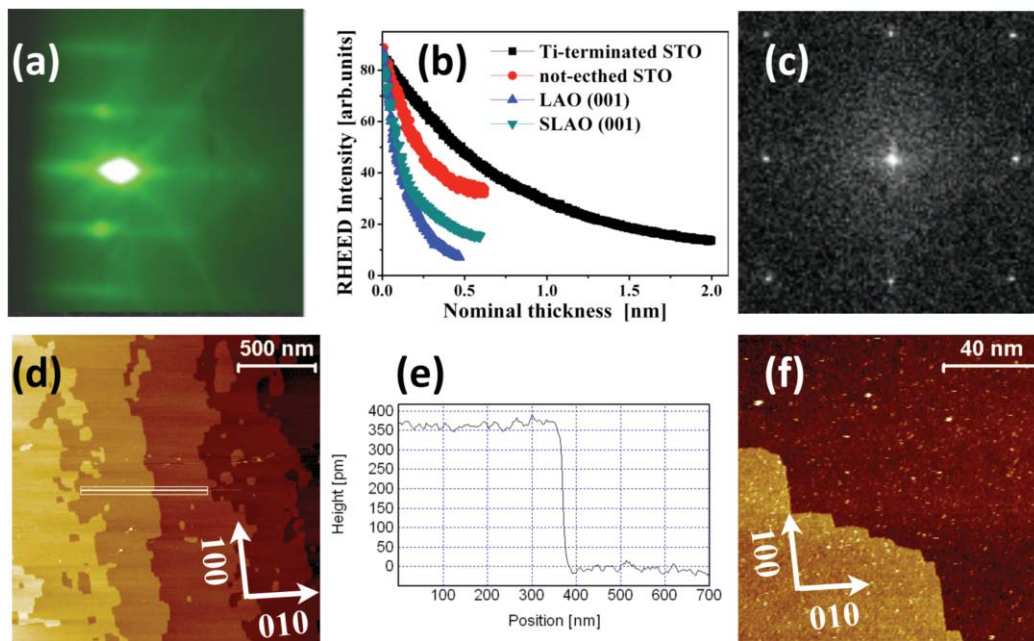| Type of substrate	STO etched (001)	STO non-etched (001)	SLAO (001)	LAO (001)
In-plane lattice parameters (nm)	0.3905	0.3905	0.3756	0.3790
Mismatch%	+3.1%	+3.1%	−0.8%	+0.1%
t_0 (nm)	0.8	0.22	<0.20	<0.20

FIG. 2. Typical (a) RHEED pattern during the early stage of deposition on Ti-terminated STO. (b) Exponential decay of the specular RHEED spot intensity vs. nominal thickness for TiO$_2$ films deposited on Ti-terminated STO (black squares), on non-etched STO (red circles), on SLAO (green down triangles), and on LAO (up blue triangles) substrates (c) LEED pattern, and (d) and (e) STM surface topography of 3 nm pseudomorphic film. RHEED and LEED patterns are unchanged with respect to the previous Ti-terminated STO surface. The terrace structure also persists, showing faceted edges along the in-plane principal directions, absent in the case of STO surfaces (e). The step profile (f) shows a vertical lattice parameter that is close to the STO c axis.

and relatively smooth surfaces (rms roughness = 2 nm on 1 × 1 μm^2 area), as confirmed by RHEED, LEED, and STM measurements.[21] TiO$_2$ films on STO (001) single crystals are characterized instead by a strikingly different behavior. In particular, the growth-mode of TiO$_2$ is strongly affected by the crystal quality and strongly depends on the atomic termination of the substrate surface.

We will now draw our attention to data obtained either on high quality surfaces of nominally TiO$_2$ terminated STO or on homo-epitaxial STO thin films. The first striking characteristic of TiO$_2$ growth on Ti-terminated STO was a steady RHEED pattern that remained qualitatively unchanged during the first nominal[23] 2–4 nm of TiO$_2$ deposition, i.e., 8–16 TiO$_2$ atomic layers (one TiO$_2$ atomic layer = 0.24 nm). In particular, the RHEED pattern was characterized by well-defined diffraction spots superimposed to diffused rods (Fig. 2(a)), indicating a 2D flat surface similar to the STO single crystal surface on which the film was deposited. The specular RHEED intensity as function of time was however not constant and followed a slow exponential decay (Fig. 2(b)),

$$I(t) = I_0 + ke^{-t/t_0}. \qquad (1)$$

The "STO-like" RHEED pattern remained unchanged until a thickness of few nanometers was deposited. The phenomenon was reproducibly found on several samples. We routinely employed the very regular RHEED oscillations of homoepitaxial STO films grown on Ti-terminated STO as an independent calibration of our laser pulse energy on the target. Such a procedure guarantees that comparable growth conditions hold for all samples. The early stage of the growth

of a TiO$_2$ on such as grown STO layers showed the same phenomenology.

This behavior is in contrast with TiO$_2$ growth on LAO and SLAO, where the RHEED specular intensity was characterized by an exponential decay much faster than the one detected on samples grown on Ti-terminated STO. This behavior is quantified by the different values of the parameter t_0 obtained from a fit of the data shown in Fig. 2(b). We find t_0 of the order of 0.15 nm (7–8 laser pulses) for films deposited on LAO and SLAO, 0.24 nm (13–14 pulses) for samples deposited on untreated STO, and up to 0.8–0.9 nm (44–50 pulses) when TiO$_2$ is deposited on TiO$_2$ terminated STO (Table I).

In order to establish the growth mode during the early stages of epitaxy, we performed systematic *in situ* studies of thin TiO$_2$ films deposited by using RHEED, LEED, SPM, and XPS techniques. RHEED (Fig. 3(a)) and LEED (Fig. 3(b)) demonstrated that TiO$_2$ thin films deposited on Ti-terminated STO are characterized by an in-plane structure indistinguishable from that one of the single crystal substrate. In particular, we observed very sharp LEED diffraction spots, which suggest an in-plane structural coherence that is comparable to that of STO. Moreover, these data allowed a precise determination of the in-plane lattice parameters, which within 1% were consistent with the square STO 2D unit cell of 0.39 × 0.39 nm^2. STM/AFM data, on the other hand, showed that the thin films are composed of well-ordered flat terraces. The height of the atomically flat terraces, being c = 0.37 ± 0.01 nm, was very surprisingly much closer to the STO c axis than to any possible characteristic distance between consecutive equivalent planes in the rutile or anatase phases of TiO$_2$. Two-dimensional islands are mostly absent, indicating that in
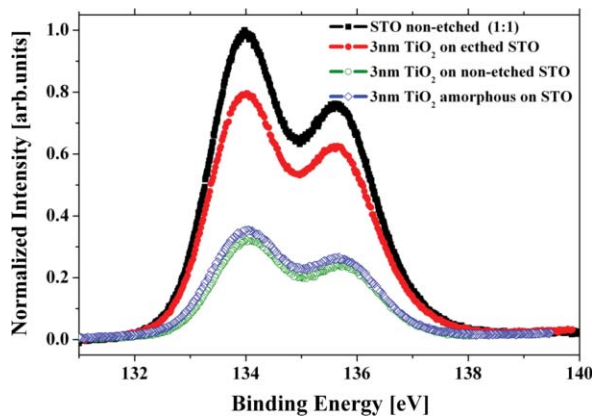
FIG. 3. (a) $3d_{5/2}$-$3d_{3/2}$ Sr peaks collected at grazing incidence for a series of samples: non-etched STO single crystal (reference sample) before (black circles), and after deposition of a nominally 3 nm thick TiO_2 film (green circles); 3nm TiO_2 film grown on TiO_2-terminated STO (red circles), 3 nm thick TiO_2 film grown at room temperature (blue circles). The intensities of all the $3d_{5/2}$-$3d_{3/2}$ Sr peaks were normalized to the $2p_{3/2}$-$2p_{1/2}$ Ti emissions. All data have been rescaled by setting the maximum of the Sr emission intensity to 1.

the early stage, TiO_2 ad-atoms are incorporated at the STO step edges [Fig. 3(c)]. These *in situ* analyses suggest that during the early stage of deposition a pseudomorphic epitaxial layer growing in step-flow mode is formed on Ti-terminated SrTiO₃. The data also show that this ultra-thin pseudomorphic film resembles a "STO-like" pseudo-cubic phase. The surface morphology, although qualitatively similar to that one of the STO substrates on which these films were grown, shows faceting along {100} and {010} directions that is not typical for STO, suggesting that {100} surfaces have the lowest surface energy. (See, for example, the growth features of homoepitaxial and heteroepitaxial STO shown in Refs. 21 and 24). Driven by an analogy with Bravais cubic lattices, we speculate that this might be attributed to a partial occupancy of the central A site of the cubic cell. Indeed, {110} surfaces have the lowest energy in BCC structures, while {100} surfaces are the lowest energy ones in simple cubic systems.

Having established that a thin epitaxial pseudomorphic film is formed during the early stage of growth, we tried to obtain information about the stoichiometry of this phase. Using XPS analyses, in particular, we obtained a semi-quantitative estimation of the Sr/Ti ratio, by comparing the integrated intensities of the Sr $3d_{5/2}$-$3d_{3/2}$ and Ti $2p_{3/2}$-$2p_{1/2}$ photoemission lines of different samples. We acquired spectra in two geometrical configurations: normal emission (90° to the substrate plane) and grazing emission (25° to the substrate plane). Note that the probe depth of the XPS technique is on the order of the film thickness (2–4 nm), even in the grazing configuration, since the expected inelastic mean free path λ of Sr $3d$ and Ti $2p$ photoelectrons (with 1119 eV kinetic energy for our Mg Kα source) is ≈2.5 nm.[25] Figure 3 shows a comparison between the Sr $3d_{5/2}$-$3d_{3/2}$ photoemission peaks, normalized to the Ti $2p$, of untreated STO single crystal (having an equal amount of Sr and Ti at the surface and in the bulk) and of a pseudomorphic 3 nm TiO_2 film deposited on a TiO_2-terminated STO (pseudomorphic phase). Data from a 3-nm anatase film (deposited on untreated STO) and from a 3-nm amorphous TiO_2 film (grown at room temperature) are also

shown for comparison. Presented XPS data (Fig. 3) are collected at grazing configuration for a series of samples. We notice that the normalized Sr signal of the pseudomorphic film is slightly lower than the one obtained in the case of SrTiO₃. On the other hand, as expected, the anatase and amorphous samples show a much lower Sr signal, which is only due to the contribution of the SrTiO₃ single crystal below. This contribution, indeed, disappears for a 10 nm thick film, which is predominately composed by a TiO_2 anatase phase.

These data show that the thin pseudomorphic layer is a Sr deficient Sr_xTiO_{2+y} pseudocubic phase. They also explain the previously discussed slow exponential decay of the real-time RHEED specular spot shown in Fig. 2. The intensity variation is only marginally related to the evolution of surface morphology, which remains mostly unchanged during the earliest phases of growth, and it presumably follows the slow evolution of the surface stoichiometry. The gradual decrease of Sr content can contribute in different ways to the decrease of the RHEED spot intensity: (i) decrease of the element with the highest scattering factor; (ii) variation of the vertical lattice parameter (decreasing from 0.39 to 0.37 nm, as shown by STM/AFM data) and consequent dephasing of electrons scattered at different depths; (iii) increase of disorder due to the presence of vacancies or substitutions.

Thus the combination of RHEED, LEED, STM, and XPS *in situ* techniques allows establishing that a Sr_xTiO_{2+y} pseudomorphic STO-like phase is realized in the early stage of PLD growth of TiO_2 films on TiO_2 terminated STO substrates. A transition to the anatase phase occurs above 10 nm. The nucleation of the TiO_2 anatase phase is easily identified by RHEED in real time with the appearance of a typical three-dimensional (3D) pattern, which shows the transition from the step-flow growth mode characteristic of the pseudomorphic STO-like phase, to a 3D island growth mode (Fig. 4, cyan line and circle).

In order to analyze more clearly the transition between pseudomorphic to anatase phase, we studied the three different stages of the deposition process (pseudomorphic, intermediate, anatase) by moving a single sample back and forth from the PLD chamber to the analytical chamber. The LEED pattern of the intermediate phase (Fig. 5(a)) is composed of sharp diffraction spots associated with a square lattice similar to the STO-like phase, but with lattice parameters about 2%–3% smaller, and a new "cross-like" structure suggestive of a sixfold reconstruction. AFM measurements (Figs. 5(b) and 5(c)) clarify that the surface is composed of small 3D-islands on top of flat terraces. Thus, in this intermediate phase, the sample is composed of a major STO-like phase and a minority of 3D islands, which on the other hand give rise to the typical 3D RHEED pattern of Fig. 4(b), due to the grazing incidence conditions. The appearance of 3D islands determines the end of the STO-like deposition phase, and the subsequent incorporation of TiO_2 ad-atoms to the island, is interpreted on the base of our data as the nucleation of a relaxed anatase. During this growth-stage the Sr migration into the film is mostly suppressed with respect to the perovskite-like phase due to the absence of available A-type sites in the TiO_2 structure. Upon further TiO_2 deposition, these islands coalesce and recover a predominant 2D surface. The anatase film is easily
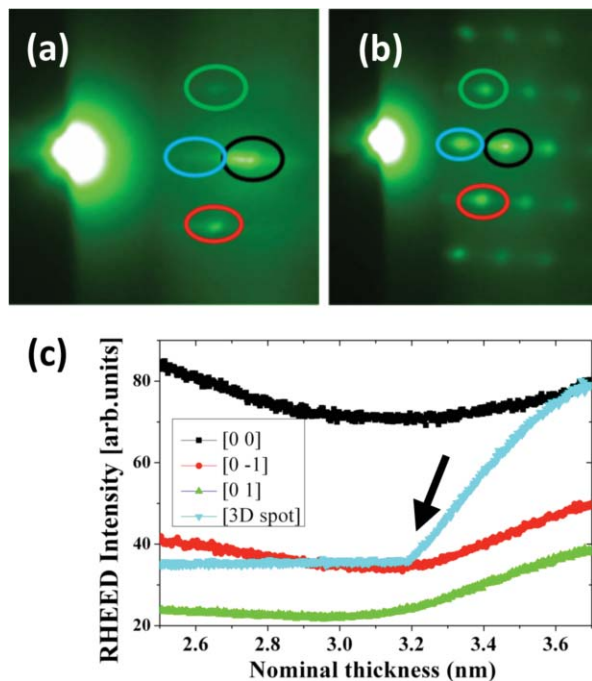
FIG. 4. RHEED patterns of a TiO$_2$ film during (a) the pseudomorphic growth of the STO-like phase and (b) during the intermediate phase where 3D anatase islands appear. In (c) the RHEED intensity of different diffraction spots as function of time is shown (the colors correspond to the circles in (a) and (b). The arrow indicates the starting of nucleation of 3D islands.

recognized from the appearance of the typical (4 × 1) surface reconstruction as shown in Fig. 6, where extensive RHEED, LEED, and STM data demonstrate that the reconstruction is related to the presence of two-domain row-like structures on the anatase surface (Fig. 6(c)). The presence of domains can be attributed to the coalescence of islands with different row alignments. A single domain area is shown in Fig. 6(d).

DISCUSSION

It is widely recognized that under reducing conditions, STO undergoes several complex chemical reactions involving defect formation and diffusion. In brief, two main processes take place. The first one is the creation of oxygen
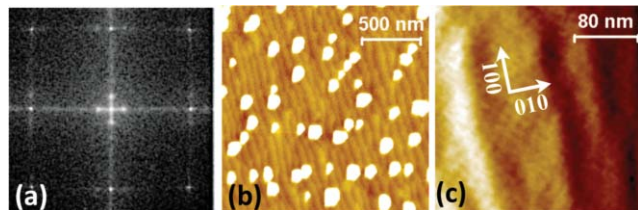

FIG. 5. (a) LEED pattern at the transition between phase B and phase C. The in-plane lattice parameter, as deduced by the dimension of the BZ, shows a ≈2%–3% reduction in real space, compatible with a partial relaxation towards the TiO$_2$ in-plane lattice parameter values. Furthermore, a cross-like structure compatible with a sixfold reconstructions is visible around the diffractions spots. (b) AFM image showing the nucleation of islands on a background surface where the presence of steps is still visible. Islands have lateral dimensions on the order of 100 nm and an average height of 3–4 nm. (c) A zoom of a region not containing the 3D islands, showing the step structure and the presence of a sixfold superstructure.
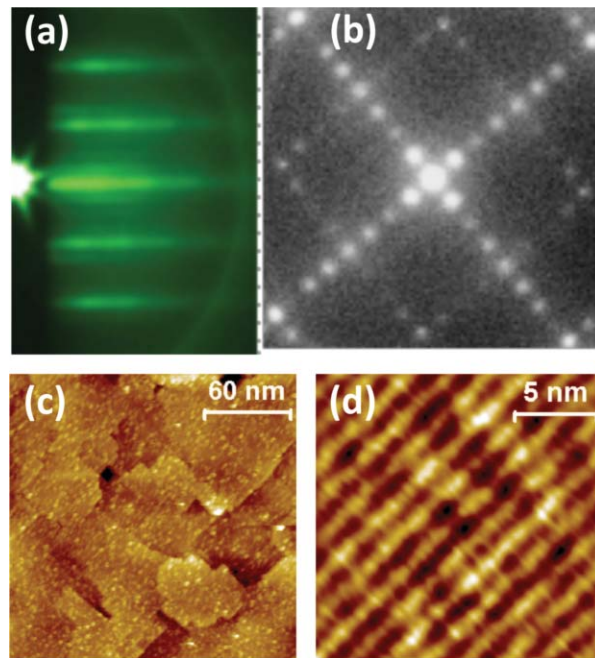

FIG. 6. (a) RHEED and (b) LEED data from 10 nm thick TiO$_2$ film deposited on SrTiO$_3$ surface. (a) The RHEED pattern is indicative of the coalescence of the islands into a uniform anatase film and shows an evident (4 × 1) reconstruction. (b) LEED pattern showing a square in-plane lattice and the presence of two perpendicular (4 × 1) reconstructed domains. The spot width demonstrates an inferior crystal quality with respect to samples grown on LAO and SLAO (not shown). (c) STM images (I$_t$ = 1 nA V$_{bias}$ = 1.0 V, 200 × 200 nm^2) showing a continuous anatase film formed by the coalescence of faceted islands. (d) High resolution STM image of a single domain area of the anatase film proves the existence of the surface reconstruction. The "row-like" structure has a periodicity of four unit cells.

vacancies.[26–28] The second, slower reaction involves the Sr cations. It was at first proposed that this is achieved by the establishment of rocksalt intergrowth layers (the Ruddlesden-Popper phases SrO$_x$(SrTiO$_3$)$_n$).[29] No experimental indication of such intergrowth in SrTiO$_3$ has, however, been found. On the contrary, overwhelming evidence indicates an alternative defect mechanism, where strontium vacancies and the SrO-rich second phase can be exclusively created at the surface of single crystals due to cation diffusion.[30–32]

Having ascertained that Sr migration occurs at the STO surface, it is possible to propose a model that accounts for the whole body of our results regarding the TiO$_2$ growth. The reaction of creations of Sr vacancies and SrO under the growth conditions may then be written as

$$\frac{1}{2}O_2(g) + 2e' + Sr^\times_{Sr} \xrightarrow{ox} V''_{Sr} + SrO, \qquad (2)$$
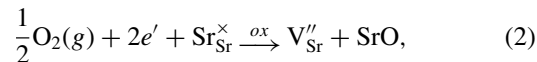
where Sr$^\times_{Sr}$ and V''$_{Sr}$ represent metal ion and metal vacancy, respectively. Under the deposition conditions, Sr vacancies are formed close to the STO surface and Sr ad-atoms appear. We believe that the growth front of the TiO$_2$ film incorporates the Sr ad-atoms in a continuous and efficient way during the growth process. When Sr diffuses in the lattice formed by a sequence of TiO$_2$ layers, the film stoichiometry is transformed into a Sr$_x$TiO$_{2+y}$ phase.

While the Sr-rich side of the Sr–Ti–O phase diagram (Sr/Ti > 1) hosts a number of theromodinamically stable

phases, such as the Ruddlesen Popper series, in bulk systems Sr doped TiO_2 separates into the anatase phase, possessing a poor Sr solubility, and $SrTiO_3$.[33] On the other hand, the local formation of a defective perovskite-like structure is possible in epitaxial non-stoichiometric $SrTiO_3$ films, forming a $SrTi_2O_5$ composition.[34] Furthermore, we believe that strain minimization is the driving force that sustains the defective pseudomorphic perovskite beyond the limits assigned by a bulk phase diagram. The capability of epitaxial growth to stabilize lattice matched phases that are not found in a bulk phase diagram has been discussed in detail in Ref. 35.

Our scenario is thus the following: during the pseudo-morphic growth, the TiO_2 ad-atoms impinging on the terraces and condensing at the edges during a step-flow growth feel a driving force to crystallize in a form that allows a three-dimensional lattice matching along the two in-plane directions and along the vertical one (step-height). Such a matching is accomplished by resorting to the available Sr atoms and the formation of the defective perovskite. Our data suggest that, through this mechanism, a relatively small amount of Sr atoms intercalated between the two terminating TiO_2 layers, together with strain minimization at the step edge, can force the growing TiO_2 layer to align with the underlying one, straightening the Ti–O–Ti bonds and forming a pseudocubic structure. Interstitial Sr is therefore immediately incorporated in the A-site cation of a defective perovskite, having the lattice parameters matched to STO with small or null elastic energy. The formation of a new perovskite layer allows in turn the formation of a fresh step edge, where segregated Sr atoms and Ti ad-atoms can react. Although the STO substrate can be regarded as an infinite Sr reservoir, the reduced Sr mobility determines an upper limit to the amount of transferred Sr atoms, and therefore, to the thickness of the intermediate, perovskite-like layer. The process will stop abruptly with the nucleation of unstrained anatase islands, which will cover the surface eventually giving rise to a uniform TiO_2 anatase film. We observe that the reported sequence of growth stages is analogous to what was recently reported during the quite different case of a metal deposited over an alloy, that is, Al on NiAl.[36] The authors found a first "steady" surface state, where in spite of the Al deposition the surface maintained the structure and stochiometry of the underlying alloy substrate, due to the flux of Ni atoms into the film. This intermediate steady state ends with the condensation of pure Al in specific surface sites, analogously to the TiO_2 islands in our films.

CONCLUSIONS

We showed that a long-range cation interdiffusion process can be activated at the anatase $TiO_2(001)/SrTiO_3(001)$ interface and that the substrate dynamically provides a flux of Sr atoms to the film. By adopting an all *in situ* approach for monitoring the surface of the growing samples by several complementary techniques, we show that the transition from the initial Ti- terminated STO surface to the final uniform TiO_2 films takes place through two intermediate phases: the growth of a strain stabilized, lattice-matched defective Sr_xTiO_{2+y} perovskite, due to the interdiffusion of Sr from the substrate, and the nucleation on the previous phase of three-dimensional relaxed anatase islands.

Our results, beside pointing out the need of resorting to alternative substrate materials for the growth of high quality anatase TiO_2 films, enrich the phase diagram of the Sr–Ti–O system under epitaxial strain opening the route to the study of the electronic and dielectric properties of the reported Sr-deficient STO phase.

[1] A. Ohtomo and H. Y. Hwang, Nature (London) **427**, 423 (2004).
[2] R. Pentcheva and W. E. Pickett, Phys. Rev. Lett. **102**, 107602 (2009).
[3] J. Mannhart, D. H. A. Blank, H. Y. Hwang, A. J. Millis, and J.-M. Triscone, MRS Bull. **33**, 1027 (2008).
[4] P. Perna, D. Maccariello, M. Radovic, U. Scotti di Uccio, I. Pallecchi, M. Codda, D. Marré, C. Cantoni, J. Gazquez, M. Varela, S. Pennycook, and F. Miletto Granozio, Appl. Phys. Lett. **97**, 152111 (2010).
[5] Scott A. Chambers, Adv. Mater. **22**, 219–248 (2010).
[6] P. K. Song, Y. Irie, and Y. Shigesato, Thin Solid Films **496**, 121 (2006).
[7] B. O'Regan and M. Grätzel, Nature (London) **353**, 737 (1991).
[8] A. M. Taurino, M. Epifani, T. Toccoli, S. Iannotta, and P. Siciliano, Thin Solid Films **436**, 52 (2003).
[9] H. Kim, G. P. Kushto, C. B. Arnold, Z. H. Kafafi, and A. Piqué, Appl. Phys. Lett. **85**, 464 (2004).
[10] S. A. Wolf, D. D. Awschalom, R. A. Buhrman, J. M. Daughton, S. von Molnár, M. L. Roukes, A. Y. Chtchelkanova, and D. M. Treger, Science **294**, 1488 (2001).
[11] M. Murakami, Y. Matsumoto, K. Nakajima, T. Makino, Y. Segawa, T. Chikyow, P. Ahmet, M. Kawazaki, and H. Koinuma, Appl. Phys. Lett. **78**, 2664 (2001).
[12] C. C. Hsieh, K. H. Wu, J. Y. Juang, T. M. Uen, J.-Y. Lin, and Y. S. Gou, J. Appl. Phys. **92**, 2518 (2002).
[13] K. A. Müller and H. Burkard, Phys. Rev. B **19**, 3593 (1979).
[14] In order to match the in-plane lattice parameters of STO, anatase will have either (a) to stretch the O-Ti-O equatorial bond angle from the equilibrium value of about 156°, or (b) to lengthen the Ti-O equatorial bond from an equilibrium value of about 0, 1934 nm. Actually, both mechanisms can be assumed to be at play.
[15] X. Weng, P. Fisher, M. Skowronski, P. A. Salvador, and O. Maksimov, J. Cryst. Growth **310**, 545 (2008).
[16] C. W. Schneider, M. Esposito, I. Marozau, K. Conder, M. Doebeli, Hu Yi, M. Mallepell, A. Wokaun, and T. Lippert, Appl. Phys. Lett. **97**, 192107 (2010).
[17] P. Blennow, K. K. Hansen, L. Reine Wallenberg, and M. Mogensen, Electrochim. Acta **52**, 1651 (2006).
[18] R. Ciancio, E. Carlino, C. Aruta, D. Maccariello, F. Miletto Granozio, and U. Scotti di Uccio, private communication (January 2011).
[19] G. Koster, B. L. Kropman, G. J. H. M. Rijnders, D. H. A. Blank, and H. Rogalla, Appl. Phys. Lett. **73**, 2920 (1998).
[20] A. Fragneto, G. M. De Luca, R. Di Capua, U. Scotti di Uccio, M. Salluzzo, X. Torrelles, T.-L. Lee, and J. Zegenhagen, Appl. Phys. Lett. **91**, 101910 (2007).
[21] M. Radovic, Ph.D. dissertation, Università degli Studi di Napoli Federico II, Italy, 2008; see http://www.fedoa.unina.it/3474/.
[22] G. S. Herman, M. R. Sievers, and Y. Gao, Phys. Rev. Lett. **84**, 3354 (2000).

[23]We are referring here to a "nominal" thickness of TiO$_2$, calibrated from the deposition rates of films deposited on LAO. It is a measure of the amount of TiO$_2$ material deposited on the substrate, not necessarily corresponding (due the interaction with the substrate) to the thickness of the pseudomorphic initial layer.

[24]M. Radovic, N. Lampis, F. Miletto Granozio, P. Perna, Z. Ristic, M. Salluzzo, C. M. Schlepütz, and U. Scotti di Uccio, Appl. Phys. Lett. **94**, 022901 (2009).

[25]G. G. Fuentes, E. Elizalde, F. Yubero, and J. M. Sanz, Surf. Interface Anal. **33**, 230 (2002).

[26]F. A. Kroger and H. J. Vink, Solid State Phys. **3**, 307 (1956).

[27]R. Waser, T. Baiatu, and K. H. Hardtl, J. Am. Ceram. Soc. **73**, 1645 (1990).

[28]J. Claus, M. Leonhardt, and J. Maier, J. Phys. Chem. Solids **61**, 1199 (2000).

[29]R. Moos and K. H. Hardtl, J. Am. Ceram. Soc. **80**, 2549 (1997).

[30]T. Ohnishi, K. Shibuya, M. Lippmaa, D. Kobayashi, H. Kumigashira, M. Oshima, and H. Koinuma, Appl. Phys. Lett. **85**, 272 (2004).

[31]K. Szot, W. Speier, U. Breuer, R. Meyer, J. Szade, and R. Waser, Surf. Sci. **460**, 112 (2000).

[32]K. Gomann, G. Borchardt, M. Schulz, A. Gomann, W. Maus-Friedrichs, B. Lesage, O. Kaitasov, S. Hoffmann-Eiferte, and T. Schneller, Phys. Chem. Chem. Phys. **7**, 2053 (2005).

[33]H. C. Ling and M. F. Yan, J. Mater. Sci. **18**, 2688 (1983)

[34]P. Fisher, H. Du, M. Skowronski, P. A. Salvador, O. Maksimov, and X. Weng, J. Appl. Phys. **103**, 013519 (2008).

[35]U. Scotti di Uccio, F. Miletto Granozio, A. Di Chiara, F. Tafuri, O. I. Lebedev, K. Verbist, and G. van Tendeloo, Physica C **321**, 162 (1999).

[36]J. P. Pierce, N. C. Bartelt, and K. F. McCarty, Phys. Rev. Lett. **99**, 026101 (2007).